POLIE suppresses telomerase-mediated telomere G-strand extension and helps ensure proper telomere C-strand synthesis in trypanosomes

M.A.G. Rabbani [1,†]**, Maiko Luis Tonini**[1,†]**, Marjia Afrin**[1] **and Bibo Li**[1,2,3,4,*]

[1]Center for Gene Regulation in Health and Disease, Department of Biological, Geological, and Environmental Sciences, College of Sciences and Health Professions, Cleveland State University, 2121 Euclid Avenue, Cleveland, OH 44115, USA, [2]Case Comprehensive Cancer Center, Case Western Reserve University, 10900 Euclid Avenue, Cleveland, OH 44106, USA, [3]Department of Inflammation and Immunity, Lerner Research Institute, Cleveland Clinic, 9500 Euclid Avenue, Cleveland OH 44195, USA and [4]Center for RNA Science and Therapeutics, Case Western Reserve University, 10900 Euclid Avenue, Cleveland, OH 44106, USA

ABSTRACT

Trypanosoma brucei **causes human African trypanosomiasis and sequentially expresses distinct VSGs, its major surface antigen, to achieve host immune evasion. VSGs are monoallelically expressed from subtelomeric loci, and telomere proteins regulate VSG monoallelic expression and VSG switching.** ***T. brucei*** **telomerase is essential for telomere maintenance, but no regulators of telomerase have been identified.** ***T. brucei*** **appears to lack OB fold-containing telomere-specific ssDNA binding factors that are critical for coordinating telomere G- and C-strand syntheses in higher eukaryotes. We identify POLIE as a telomere protein essential for telomere integrity. POLIE-depleted cells have more frequent** ***VSG*** **gene conversion-mediated VSG switching and an increased amount of telomeric circles (T-circles), indicating that POLIE suppresses DNA recombination at the telomere/subtelomere. POLIE-depletion elongates telomere 3′ overhangs dramatically, indicating that POLIE is essential for coordinating DNA syntheses of the two telomere strands. POLIE depletion increases the level of telomerase-dependent telomere G-strand extension, identifying POLIE as the first** ***T. brucei*** **telomere protein that suppresses telomerase. Furthermore, depletion of POLIE results in an elevated telomeric C-circle level, suggesting that the telomere C-strand experiences replication stress and that POLIE may promote telomere C-strand synthesis. Therefore,** ***T. brucei*** **uses a novel mechanism to coordinate the telomere G- and C-strand DNA syntheses.**

INTRODUCTION

Telomeres are nucleoprotein complexes at chromosome ends and are essential for genome integrity and chromosome stability (1,2). In most eukaryotes, telomeres consist of simple repetitive sequences with the TG-rich strand running 5′ to 3′ towards the chromosome end (3) and terminate with a 3′ single-stranded overhang structure (4). Conventional DNA polymerases cannot fully replicate the ends of linear DNA molecules, resulting in progressive telomere shortening in proliferating cells (5,6). In most eukaryotes, a specialized reverse transcriptase, telomerase, can synthesize the telomere G-rich strand *de novo*, effectively solving this 'end replication problem' (7,8). Telomerase contains a protein catalytic subunit with a reverse transcriptase activity, TERT, and a template-harboring RNA subunit, TR (7,8). Telomerase uses a G-rich single-stranded 3′ DNA end as its substrate (9,10). Hence, the telomere 3′ overhang is essential for telomerase-mediated telomere extension (4). The telomere 3′ overhang can also invade the duplex telomere region of the same telomere to form the T-loop structure (11), which helps protect the telomere from illegitimate nucleolytic degradation and DNA damage repair processes (2). Therefore, the telomere 3′ overhang structure is essential for telomere maintenance and chromosome end protection.

Generation of a proper telomere 3′ overhang structure takes several steps and is tightly regulated by several telomere proteins (4,12). After DNA replication by conventional DNA polymerases in the S phase, the leading strand telomere synthesis results in a blunt-ended product while the

---

lagging strand telomere synthesis results in a short 3′ overhang after removing the 5′ RNA primer. In mammalian cells, Apollo, a 5′ to 3′ exonuclease, resects the 5′ end of the leading strand product (13), then Exo1 further resects the 5′ ends of both leading and lagging strand products (14,15). Subsequently, telomerase acts on the telomere 3′ overhang to elongate the telomere G-strand (9). Finally, a DNA polymerase, such as DNA polymerase alpha-primase in mammals, finishes the C-strand fill-in (16). In vertebrates, yeasts, and plants, OB fold-containing telomere ssDNA binding proteins such as the POT1/TPP1 complex (17–20) and the CST complex (vertebrate CTC1/budding yeast CDC13, STN1, and TEN1) (21–24) play critical roles in coordinating the telomere G-strand extension and C-strand fill-in (25). For example, the human TPP1/POT1 complex binds the telomere 3′ overhang through POT1 (26,27) and recruits telomerase to the telomere and stimulate telomerase activity through TPP1 (28–30). In addition, binding of the CST complex on the telomere 3′ overhang effectively inhibits telomerase-mediated telomere extension (31). Similarly, in budding yeasts, CDC13, the single-stranded telomere DNA binding factor, both positively and negatively regulates telomerase-mediated telomere extension: CDC13 interacts with EST1, a telomerase accessory protein, to help recruit telomerase to the telomere (32). However, the binding of the CST complex (CDC13/STN1/TEN1) to the telomere also prevents the access of telomerase to the telomere substrate (33). Furthermore, both vertebrate and yeast CST promotes the telomere C-strand fill-in by directly interacting with and recruiting DNA polymerase alpha-primase to the telomere (23,25,34–36). Therefore, telomere ssDNA binding factors are major players to coordinate the synthesis of the two telomere strands. However, OB fold-containing telomere-specific ssDNA binding factors have not been identified in *Trypanosoma brucei*, and telomere end processes are poorly understood in this organism.

Trypanosoma brucei is a protozoan parasite that causes human African trypanosomiasis. While proliferating in its mammalian host, bloodstream form (BF) *T. brucei* sequentially expresses immunologically distinct variant surface glycoproteins (VSGs), its major surface antigen, to evade the host immune response. *T. brucei* has a large *VSG* gene pool with most *VSGs* in large subtelomeric *VSG* arrays (37), and VSG is expressed exclusively from ∼15 subtelomeric expression sites (ESs) in a strictly monoallelic manner (38,39). Telomerase-mediated telomere synthesis is the predominant mechanism of telomere maintenance in *T. brucei* (40–42). *T. brucei* telomeres also form a T-loop structure (43). In addition, *T. brucei* telomere has a short G-rich 3′ overhang (44,45). The telomere structure and telomere proteins are not only essential for *T. brucei* genome stability and cell proliferation but are also essential for monoallelic *VSG* expression and regulate the VSG switching frequency (46–58). We previously found that *T. brucei* has very short telomere 3′ overhangs (∼12 nts) (44,45), suggesting that the telomere C-strand fill-in is well-coordinated with the G-strand extension. However, the OB fold-containing telomere-specific ssDNA binding factors appear to be absent in the *T. brucei* genome, and so far no telomerase regulators have been identified. Rather, a zinc finger-containing

protein UMSBP2 that is important for mitochondrial DNA replication can bind the G-rich telomere ssDNA (59,60). Depletion of UMSBP2 leads to a decreased G-rich but an increased C-rich ssDNA signal level and an increased amount of telomeric circles (60).

Here, we performed both Proteomics of Isolated Chromatin Segments (PICh) (61) of the telomere chromatin and affinity pulled-down the telomere protein complex. We have identified POLIE as an intrinsic component of the *T. brucei* telomere complex that is essential for telomere integrity and suppresses DNA recombination at the telomere and subtelomere. Depletion of POLIE elongates telomere 3′ overhangs dramatically, indicating that POLIE helps coordinate telomere G- and C-strand syntheses. Interestingly, we detected a higher level of telomerase-dependent telomere G-strand extension in POLIE-depleted cells, identifying POLIE as the first telomere protein that suppresses telomerase in *T. brucei*. In addition, the increased telomeric C-circle level in POLIE-depleted cells suggests that these cells experience telomere C-strand replication stress and that POLIE also helps ensure telomere C-strand synthesis.

MATERIALS AND METHODS

T. brucei strains

All *T. brucei* strains used in this study are listed in Table 1. Generation of $TRF^{F2H+/-} TIF2^{+F2H/-}$: Procyclic form (PF, the insect stage) *T. brucei* WT cells (Lister 427) were transfected with pSK-TRF-ko-*Hyg* (46) and pSK-TIF2-ko-*BSD* (49) to delete one allele of *TRF* and *TIF2*, respectively. The resulting cells were transfected with pSK-F2H-TRF-*Pur*-tar and pSK-TIF2-F2H-*Phleo*-tar (49) to insert the FLAG-HA-HA (F2H) tag to the N- and the C-terminus of the remaining allele of *TRF* and *TIF2*, respectively.

All bloodstream form (BF, the life cycle stage when *T. brucei* resides in a mammalian host) *T. brucei* strains used in this study were derived from VSG2-expressing Lister 427 cells that express the T7 polymerase and the Tet repressor (Single Marker, aka SM) (62). The HSTB261 strain is derived from SM and specifically designed for assaying VSG switching (63), which we renamed as the S strain for easier reference (49). SM, $TIF2^{+F2H/+}$ (49), and the S cells were transfected with pSK-POLIE-myc13-*Hyg*-tar to tag one endogenous allele of *POLIE* with a C-terminal 13 × myc. $POLIE^{+myc/+}$ cells were transfected with pZJMβ-TRF (46) and pZJMβ-POLIE to generate $POLIE^{+myc/+}$ TRF RNAi and $POLIE^{+myc/+}$ RNAi, respectively. The S cells were transfected with pZJMβ-POLIE to generate S/IEi followed by transfection with pSK-POLIE-myc13-*Hyg*-tar to generate $POLIE^{+myc/+}$ S/IEi. S/IEi cells were also transfected with pLew100v5-POLIE-myc to generate S/IEi + ecPOLIE-myc. $TR^{-/-}$ cells (41) were transfected with pZJMβ-POLIE to generate $TR^{-/-}$ POLIE RNAi. SM and $POLIE^{+myc/+}$ cells were transfected with pSK-POLIE-ko-*BSD* to generate $POLIE^{+/-}$ and $POLIE^{+myc/-}$.

Plasmids

A 500 bp genomic DNA fragment upstream of the *TRF* gene, the *Puromycin resistance* gene (*PUR*), the α/β tubu-

Table 1. List of *T. brucei* strains used in this study

Strain	Life cycle stage & description of genotype
$TRF^{F2H+/-} TIF2^{+F2H/-}$	PF; one allele of *TRF* is deleted and the other is N-terminally FLAG-HA-HA (F2H)-tagged; one allele of *TIF2* is deleted and the other is C-terminally F2H-tagged
$POLIE^{+myc/+}$	BF; one allele of *POLIE* is C-terminally tagged with 13 x myc
$POLIE^{+/-}$	BF; one allele of *POLIE* is deleted
$POLIE^{+myc/-}$	BF; one allele of *POLIE* is C-terminally tagged with 13 x myc and the other is deleted
$POLIE^{+myc/+} TIF2^{+F2H/+}$	BF; one allele of *POLIE* is C-terminally tagged with 13 x myc; one allele of *TIF2* is C-terminally tagged with F2H
$POLIE^{+myc/+}$ TRF RNAi	BF; one allele of *POLIE* is C-terminally tagged with 13 x myc; the Tet-inducible TRF RNAi expressing construct is integrated into an rDNA spacer
$POLIE^{+myc/+}$ RNAi	BF; one allele of *POLIE* is C-terminally tagged with 13 x myc; the Tet-inducible POLIE RNAi expressing construct is integrated into an rDNA spacer
S (63)	BF; in the active *VSG2*-containing ES, a *BSD* marker is inserted immediately downstream of the ES promoter, a *PUR-TK* marker is inserted immediately upstream of the *VSG2* gene (Supplementary Figure S3A)
S/ev (49)	BF; the active ES has the *BSD* and *PUR-TK* markers; the empty RNAi construct is integrated into an rDNA spacer
S/IEi	BF; the active ES has the *BSD* and *PUR-TK* markers; the Tet-inducible POLIE RNAi expressing construct is integrated into an rDNA spacer
$POLIE^{+myc/+}$ S/IEi	BF; the active ES has the *BSD* and *PUR-TK* markers; the Tet-inducible POLIE RNAi expressing construct is integrated into an rDNA spacer; one allele of *POLIE* is C-terminally tagged with 13 x myc
S/IEi + ecPOLIE-myc	BF; the active ES has the *BSD* and *PUR-TK* markers; the Tet-inducible POLIE RNAi expressing construct is integrated into an rDNA spacer; an inducible ectopic *POLIE-myc* expressing construct is integrated into an rDNA spacer
$TR^{-/-}$ (41)	BF; both *TR* alleles are deleted
$TR^{-/-}$ POLIE RNAi	BF; both *TR* alleles are deleted; the Tet-inducible POLIE RNAi expressing construct is integrated into an rDNA spacer

lin intergenic sequence, the F2H tag, and a 500 bp fragment of the *TRF* gene (encoding its N-terminus) are inserted into pBluescript SK in this order to generate pSK-F2H-TRF-*Pur*-tar.

A 400 bp *POLIE* gene fragment (encoding its C-terminus), a 13 × myc tag, the α/β tubulin intergenic sequence, the *Hygromycin resistance* gene (*HYG*), and a 500 bp genomic DNA fragment downstream of the *POLIE* gene were inserted into pBluescript SK in this order to generate pSK-POLIE-myc13-*Hyg*-tar.

A 470 bp DNA fragment at the N-terminus of *POLIE* ORF and a 520 bp DNA fragment at the C-terminus of *POLIE* ORF were inserted into pZJMβ in tandem to generate pZJMβ-POLIE RNAi construct.

The *Blasticidin-resistance* gene (*BSD*) flanked by genomic DNA fragments upstream and downstream of the *POLIE* gene, respectively, were inserted into pBluescript SK to make pSK-POLIE-ko-*BSD*.

The DNA fragment encoding the full-length POLIE and a C-terminal 13 × myc tag were inserted into pLew100v5 to generate pLew100v5-POLIE-myc.

Nuclear fractionation and two-step immunoprecipitation

5×10^{10} $TRF^{F2H+/-} TIF2^{+F2H/-}$ PF cells were harvested by centrifugation followed by snap freezing in liquid nitrogen. After thawing cells, the cell pellet was resuspended in the hypotonic buffer (10 mM HEPES pH 7.9; 10 mM KCl; 2.5 mM MgCl$_2$; 1 mM EDTA; 1 mM DTT; Complete protease inhibitors (Roche), 1 mM PMSF, 1 μg/ml Leupeptin, 0.5 mg/ml TLCK, and 1 μg/ml Pesptatin A) and incubated on ice for 10 min followed by adding 0.2% NP-40. Cells were homogenized in a glass douncer until ~80% of the cells

were broken. The lysate was overlaid on top of 0.3 ml of sucrose buffer (0.8 M sucrose in hypotonic buffer) and centrifuged at 7 krpm for 10 min at 4°C. After removing the top cytosolic and sucrose layers, the nuclear fraction was resuspended in the TBS buffer (50 mM Tris–HCl, pH 7.4; 420 mM NaCl; Complete protease inhibitors (Roche), 1 mM PMSF, 1 μg/ml Leupeptin, 0.5 mg/ml TLCK and 1 μg/ml Pepstatin A) and digested with Benzonase on ice for 20 min followed by centrifugation at 13 krpm for 10 min at 4°C. The cell lysate was diluted with 50 mM Tris–HCl, pH 7.4 so that the final concentration of NaCl reached 150 mM. The cell lysate was pre-cleared with Dynabeads Protein G (ThermoFisher) then incubated with Anti-FLAG M2 magnetic beads (Sigma) for 3 h at 4°C. The IP product was washed 3 times with TBS-T (50 mM Tris–HCl, pH7.4; 150 mM NaCl, 0.1% Tween 20) and eluted at room temperature with 0.6 mg of the FLAG peptide. The eluate was incubated with Dynabeads Protein G conjugated with the HA monoclonal antibody 12CA5 (MSKCC Antibody & Bioresource Core Facility) for 2 h at 4°C. The IP product was washed three times with TBS-T, eluted with 0.1 M glycine, pH 2.2 at 56°C followed by neutralization with 1 M Tris–HCl pH 9.5. The final eluate was concentrated with StrataClean resin (Agilent) before extraction using 2× SDS buffer and separated in a 10% SDS-PAGE gel (Bio-Rad). The gel was stained with colloidal Coomassie brilliant blue followed by mass spectrometry analysis at the Cleveland Clinic Proteomics and Metabolomics Core. Proteins identified with at least two peptide hits were saved for further analyses. Proteins identified from WT cells were considered as the background noise and were eliminated from those identified in the $TRF^{F2H+/-} TIF2^{+F2H/-}$ cells.

Proteomics of isolated chromatin segments (PICh)

PICh was performed according to (61) with modifications. 5×10^{10} WT PF cells were harvested and washed with $1 \times$ PBS and HLB (10 mM HEPES pH 7.9; 10 mM KCl; 2.5 mM $MgCl_2$; 1 mM EDTA; 1 mM DTT; Complete protease inhibitors (Roche), 1 mM PMSF, 1 μg/ml Leupeptin, 0.5 mg/ml TLCK and 1 μg/ml Pesptatin A). Cells were resuspended in HLB, incubated on ice for 10 min, and homogenized with five strokes using a glass douncer. After adding 15% paraformaldehyde in HLB, 15–20 more strokes were performed. The lysate was centrifuged at 15 000 g in a swing bucket centrifuge at room temperature for 20 min, and the pellet was resuspended in 3% paraformaldehyde/$1 \times$ PBS with rotation for 15 min followed by three washes using $1 \times$ PBS. The pellet was then washed with the sucrose buffer (0.3 M Sucrose; 10 mM HEPES–NaOH, pH 7.9; 1% Triton-X100; 2 mM MgOAc), resuspended in the sucrose buffer and homogenized in a douncer with 20 strokes, then centrifuged at 15 000 g for 20 min at room temperature. Subsequently, the pellet was washed with $1 \times$ PBS/0.5% Triton X-100, resuspended in $1 \times$ PBS/0.5% Triton X-100/200 μg/ml RNAse A with rotation for 2 h. After two washes with $1 \times$ PBS and one wash with HSLB (10 mM HEPES–NaOH, pH 7.9; 100 mM NaCl; 2 mM EDTA; 1 mM EGTA; 0.2% SDS; 0.1% sodium sarkosyl; 1 mM PMSF), the pellet was resuspended in HSLB and incubated at room temperature for 15 min, followed by sonication for 13 cycles (30 s on/off) at maximum intensity in a Bioruptor 300 (Diagenode). Samples were heated to 58°C for 5 min in a Thermomixer, then spun down at 20 krpm for 15 min at room temperature. The supernatant was rotated for 2 h with pre-equilibrated High Capacity Streptavidin Agarose Resin slurry (Thermo). Then the mixture was centrifuged for 2 min and the supernatant was desalted by filtration with a Sephacryl S-400 HR column (GE Healthcare), centrifuged at 16 krpm, followed by adding SDS to a final concentration of 0.02%. The resulting desalted soluble chromatin was divided into two equal aliquots to which either a telomere specific [TelG, 5′ TTAGGGTTAGGGTTAGGGTTAGGGT 3′] or a scrambled (Scr, 5′ GATGTGGATGTGGGATGTG GATGTGG 3′) LNA probe was added. Chromatin and LNA probes were hybridized in a thermocycler (25°C/3 min, 71°C/9 min, 38°C/60 min, 60°C/3 min, 38°C/30 min, 25°C final temperature), then centrifuged, immunoprecipitated, eluted and TCA concentrated. Crosslink reversal was done by suspending the pellet in LDS NuPAGE sample buffer + 0.5 M 2-mercaptoethanol and incubating at 99°C for 25 min. Protein samples were resolved in 4–12% NuPAGE Bis-Tris gels (ThermoFisher), stained with colloidal Coomassie brilliant blue and stored in sealed packages until mass spectrometry analysis. Proteins identified with at least two peptide hits were saved for further analyses. Proteins identified using the control probe were considered as the background noise and removed from those identified using the $(TTAGGG)_4$ LNA probe.

EMS clonogenic survival assay

BF $POLIE^{+myc/+}$ RNAi cells were grown with or without doxycycline for 24 h then incubated with 2 mM of ethyl-methanesulfonate (EMS; Sigma) or DMSO (vehicle) for 2 h. Cells were washed three times with warm media and plated at a concentration of 1 cell/well in 96-well plates followed by incubation at 37°C. Plating efficiency was calculated as number of survival clones/total number of wells. Relative survival rates were calculated as plating efficiency of EMS treated/plating efficiency of DMSO-treated control for induced and uninduced POLIE RNAi cells.

UV and cisplatin sensitivity tests

$POLIE^{+myc/+}$ RNAi cells were incubated with and without doxycycline for 12 h then diluted to a concentration of 1.5×10^6 cells/ml. Cells were irradiated by 0, 50 J m^{-2}, or 100 J m^{-2} UV using the Stratalinker® UV Crosslinker (Stratagene) or incubated with or without 20 μM cisplatin (Sigma) for 1 h. Cells were washed free of doxycycline and cisplatin after the treatment and cell growth was monitored daily with necessary dilutions. Cell relative growth was calculated using the following formula for cells incubated with and without doxycycline: population doubling (UV/cisplatin treated)/population doubling (untreated).

VSG switching assay

Cells were maintained in the presence of blasticidin and puromycin until the start of the assay, when doxycycline was added to induce POLIE RNAi for 30 h. Cells were grown for a total of 10.5 population doublings before they were harvested. Switchers were enriched by passing cells through a VSG2 antibody-conjugated MACS column and collecting the flow through. To determine plating efficiency, cells were plated at 1 cell/well in $3 \times$ 96-well plates without ganciclovir (GCV) selection. Switchers were selected by 4 μg/ml GCV after they were diluted and distributed in multiple 96-well plates. GCV-resistant switchers were further verified by western dot-blot analysis using a VSG2 antibody. The VSG switching rate was calculated by dividing the number of switchers by the total number of cells at the time of harvesting and by the number of population doublings and was further normalized by the plating efficiency. To determine the switching mechanisms, switchers were analyzed for their sensitivity to 5 μg/ml and 100 μg/ml blasticidin and 2 μg/ml puromycin. The presence of the *BSD* and *VSG2* genes was determined by PCR using genomic DNA isolated from the switchers.

Quantitative real-time PCR (qPCR)

For qPCR, total RNA was isolated from *T. brucei* cells using RNAstat-60 (TelTest, Inc.), treated by DNase (Qiagen), and purified using the RNeasy column (Qiagen). cDNA was synthesized using a random hexamer and the MMLV reverse transcriptase (Promega) according to the manufacturer's manual. cDNA and γH2A ChIP product were analyzed by qPCR on a CFX Connect (Bio-Rad) using SsoAdvanced Universal SYBR® Green Supermix (Bio-Rad) according to the manufacturer's manual. qPCR primer sequences are listed in Supplementary Table S6.

Immunofluorescence analysis (IF)

IF was performed exactly the same way as described in (64).

Two-dimensional gel electrophoresis

5 μg of MboI/AluI digested genomic DNA were separated in the first dimension in a 0.4% agarose 1× TBE gel without EtBr under 40 volts for 18 h at room temperature. Subsequently, the gel was incubated in 1× TBE/0.3 μg/ml EtBr for 20 min followed by washing with 1× TBE. DNAs were then excised from the gel, transferred to a second 1.1% agarose gel with 1× TBE/0.3 μg/ml EtBr, and electrophoresed under 150 V at 4°C for 5 h.

The telomeric C-circle (G-circle) assay

The Φ29-mediated rolling-circle assay was performed according to (65) with minor modifications. 8 μg of AluI, MboI, and DNase-free RNase A digested genomic DNA was digested by λ Exonuclease and Exonuclease I to remove dsDNA. 20 ng of the resulting DNA was incubated with 7.5 U Φ29 DNA polymerase (NEB) in reaction buffer [1 μg/μl BSA, 0.05% Tween 20, 0.5 mM dATP, 0.5 mM dGTP (or 0.5 mM dCTP for detecting G-circles) and 0.5 mM dTTP, 1× Φ29 Buffer] at 30 °C for 8 h, then Φ29 was heat-inactivated at 65 °C for 20 min. The reaction products were slot blotted onto a Hybond N nylon membrane (GE Healthcare) followed by hybridization at 50°C with end-labeled (CCCTAA)$_4$ to detect C-circles or (TTAGGG)$_4$ to detect G-circles.

Native in-gel hybridization

Genomic DNA was treated with or without Exo I (NEB) and digested with MboI and AluI. An equal amount of ExoI treated and non-treated DNA was separated by agarose gel electrophoresis. The DNA-containing agarose gel was dried at room temperature and hybridized with an end-labeled (CCCTAA)$_4$ or (TTAGGG)$_4$ probe at 50°C. After exposing the hybridized gel to a phosphorimager, the gel was denatured, neutralized, and hybridized with the same oligo probe at 55°C followed by exposure to a phosphorimager. The hybridization signals were quantified using ImageQuant. The telomere 3′ overhang level was calculated by dividing the amount of native hybridization signal by the amount of post-denaturation hybridization signal. Alternatively, DNA plugs were prepared according to (46). Intact *T. brucei* chromosomes were separated by pulsed-field gel electrophoresis according to (49). The DNA-containing gel was dried and hybridized with the (CCCTAA)$_4$ or (TTAGGG)$_4$ probe the same way as described above.

EdU-labeling

Exponentially growing BF *T. brucei* cells (0.7–0.9 × 10^6 cells/ml) were incubated with 150 μM 5-ethynyl-2'-deoxyuridine (EdU) (Click Chemistry Tools) for 3 h before genomic DNA was isolated. DNA was sonicated to 400–1000 bp fragments. EdU-labeled DNA fragments were conjugated with desthiobiotin using the Click chemistry reagent (2 mM desthiobiotin-Azide, 100 mM/500 mM CuSO$_4$/THPTA, 50 mM Na-Ascorbate, 100 mM HEPES pH 7 and 10% DMSO). The desthiobiotin conjugated DNA was pulled-down using streptavidin beads (ThermoFisher) and eluted from the beads using biotin. The eluted DNA was dot-blotted onto a Hybond N nylon membrane (GE Healthcare) and hybridized with telomere and tubulin probes at 65°C. The blot was exposed to a phosphorimager and the signals were quantified using ImageQuant.

Strand-specific telomere probe preparation

The radioactive (CCCTAA)$_n$ probe was synthesized by Klenow using an 800 bp TTAGGG repeat dsDNA as the template and a random hexamer as the primer. Only dATP, dTTP, and radioactive dCTP were included in the reaction. The radioactive (TTAGGG)$_n$ probe was similarly synthesized except dATP, dTTP and radioactive dGTP were included in the reaction.

RNAseq and data analysis

Total RNA was isolated and purified through RNeasy columns (Qiagen) from *POLIE*$^{+myc/+}$ RNAi cells before and after 30 h of RNAi induction with two biological replicates. All RNA samples were run on a BioAnalyzer 2100 (Agilent Technologies) using the Agilent RNA 6000 nano kit to verify the RNA quality before they were sent to Novogene for library preparation and RNA high throughput sequencing followed by bioinformatic analysis the same way as described in (52).

RESULTS

Identifying *T. brucei* telomere components by PICh and TRF/TIF2 IP

We have identified several Shelterin homologs but not OB fold-containing telomere-specific ssDNA binding factors in *T. brucei* (46,47,49). In search of additional telomere factors, we first pulled-down the telomere complex through known telomere proteins, TRF (46) and TIF2 (49). We deleted one allele of *TRF* and *TIF2* and tagged the other with a FLAG-HA-HA epitope in the procyclic form (PF, the insect stage) *T. brucei* cells to establish the *TRF*$^{F2H+/-}$*TIF2*$^{+F2H/-}$ strain (Table 1). In the *TRF*$^{F2H+/-}$*TIF2*$^{+F2H/-}$ and WT cells (as a negative control), nuclear extracts were sequentially immunoprecipitated (IPed) with the FLAG monoclonal antibody M2 and HA monoclonal antibody 12CA5, and the final IP products were analyzed by mass spectrometry (Supplementary Figure S1, left). We also isolated the telomere chromatin by Proteomics of Isolated Chromatin segments (PICh) (61). Using labeled LNA probes containing either the (TTAGGG)$_4$ sequence or a scrambled sequence (as a negative control), we pulled-down the telomere chromatin and analyzed its protein components by mass spectrometry (Supplementary Figure S1, right). IP and PICh identified >800 proteins each (Tables S1–S4), and 282 proteins were identified in both (Figure 1A, Supplementary Table S5), which are considered meaningful hits. Among these, DNA polymerase IE (POLIE, Tb927.11.5550; Uniprot Accession: Q385L3) (66,67) is one of the most abundant. In a previous independent F2H-TRF pull-down experiment
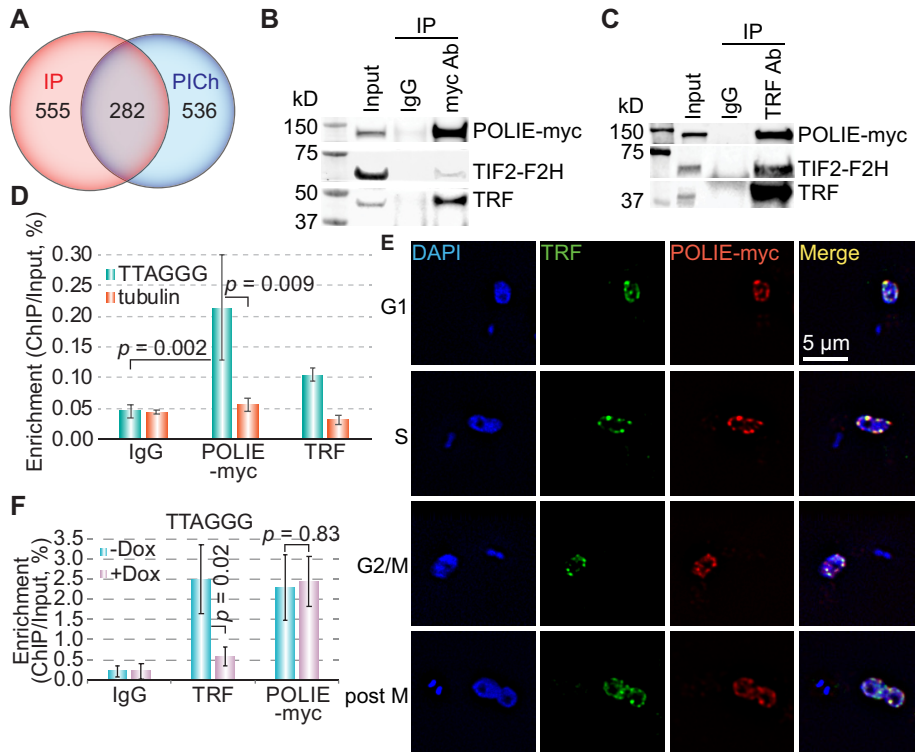
Figure 1. POLIE is an intrinsic component of the *T. brucei* telomere complex. (**A**) Venn diagram showing the number of protein candidates identified in IP of the TRF/TIF2 protein complex and in PICh. (**B & C**) IP using the myc antibody 9E10 (MSKCC Antibody & Bioresource Core Facility) (**B**) and a TRF rabbit antibody (46) (**C**) or IgG (as a negative control in both) in $POLIE^{+myc/+}$ $TIF2^{+F2H/+}$ cells. Western analyses were performed using the myc antibody 9E10, the HA antibody (HA probe, Santa Cruz Biotechnologies), and a TRF chicken antibody (47). (**D**) Quantification of ChIP results using the myc antibody 9E10, a TRF rabbit antibody (46), and IgG (as a negative control) in $POLIE^{+myc/+}$ cells. Average enrichment (ChIP/Input) was calculated from three to four independent experiments. (**E**) IF in $POLIE^{+myc/+}$ cells using the myc antibody 9E10 and a TRF rabbit antibody (46). DNA was stained with DAPI. All panels are of the same scale and the size bar is shown in one panel. Representative cells in various cell cycle stages are shown. (**F**) Quantification results of POLIE-myc and TRF ChIP in $POLIE^{+myc/+}$ TRF RNAi cells before (-Dox) and after (+Dox) the induction of TRF RNAi. Average enrichment (ChIP/Input) was calculated from three independent experiments. *P* values of unpaired *t*-tests are shown in (D) and (F). In this and other figures, error bars represent standard deviation.

(49), we also identified POLIE as one of the most abundant proteins in the TRF complex, prompting us to continue to characterize POLIE's telomere functions. In addition, we have identified *T. brucei* TRF (46), TIF2 (49), RAP1 (47), Ku70/80 (68,69), UMSBP2 (60), PIP5Pase (70), TDP1 (71), VEX1 (72), NUP98, NUP96, NUP152, SMC1, SMC3, SMC4, PPL2 (66,73), TelAP1 (66), all core histones, H3v, H4v, H2AZ and H2BV in the telomere PICh.

T. brucei POLIE is an intrinsic telomere component and suppresses VSG switching by maintaining telomere integrity

To verify that POLIE is an intrinsic component of the telomere complex, we tagged one endogenous *POLIE* allele with a C-terminal 13× myc tag and established BF *T. brucei* $POLIE^{+myc/+}$, $POLIE^{+/-}$ and $POLIE^{+myc/-}$ strains (Table 1). These and WT cells grew at nearly identical rates (Supplementary Figure S2A). $POLIE^{+myc/-}$ also has a WT telomere 3′ overhang structure (see below, Supplementary Figure S6), indicating that POLIE-myc is functional. In $POLIE^{+myc/+}$ $TIF2^{+F2H/+}$ cells (Table 1, Supplementary Figure S2B), IP of POLIE-myc using the myc monoclonal antibody 9E10 pulled-down TIF2-F2H and TRF (Figure 1B). Similarly, POLIE-myc and TIF2-F2H were present in the

TRF IP (Figure 1C), confirming that POLIE, TRF and TIF2 are in the same protein complex. In $POLIE^{+myc/+}$ cells, we performed ChIP using the myc antibody and observed that POLIE-myc is associated with the telomere chromatin (Figure 1D; S2C). We also performed the Immunofluorescence (IF) analysis in $POLIE^{+myc/+}$ cells using the myc and TRF antibodies (46). TRF is almost always colocalized with the telomere in the combined IF/FISH analysis (46). Hence, TRF was stained to mark the telomere. POLIE-myc was colocalized with TRF throughout the cell cycle (Figure 1E). These observations confirm that POLIE is an intrinsic component of the telomere complex. We further investigated whether the association of POLIE with the telomere chromatin depends on TRF, which has a duplex telomere DNA binding activity (46). ChIP was performed in $POLIE^{+myc/+}$ TRF RNAi cells (Table 1) before and after induction of TRF RNAi for 24 hrs, and ChIP products were hybridized with telomere and tubulin probes. TRF was successfully depleted from the telomere chromatin (Figure 1F; Supplementary Figure S2, D–F). However, POLIE still remained at the telomere after TRF depletion (Figure 1F; Supplementary Figure S2, D–F). Therefore, POLIE is localized to the telomere independent of TRF.

To examine functions of POLIE, we introduced the inducible POLIE RNAi construct into the *POLIE*[+myc/+] cells to establish the *POLIE*[+myc/+] RNAi strain (Table 1). Significant depletion of POLIE-myc (Figure 2A) and a growth arrest by 24 h (Figure 2B) were observed upon induction of POLIE RNAi by doxycycline, confirming that POLIE is essential for cell proliferation (67). POLIE is an A family DNA polymerase, homologous to the mammalian Polθ and Polν within their C-terminal DNA polymerase domains (67), while Polθ and Polν play important roles in DNA damage repair (74,75). Therefore, we examined whether POLIE-depleted cells were sensitive to DNA damaging agents. In the *POLIE*[+myc/+] RNAi cells, RNAi was induced for 0 and 24 h followed by treatment with 2 mM EMS (a DNA alkylating agent) for 2 h, and a clonogenic survival assay was performed. Cells depleted of POLIE exhibited a significantly reduced survival rate than uninduced cells (Figure 2C). In addition, *POLIE*[+myc/+] RNAi cells were induced for 12 h and incubated with cisplatin (causes interstrand crosslinks) or irradiated with UV light (causes cyclobutane pyrimidine dimers), and cell growth was monitored (Supplementary Figure S2G, H). Cells treated with cisplatin had a poorer relative growth (treated/untreated) in POLIE RNAi induced cells than in uninduced cells (Figure 2D). Similarly, after UV irradiation, the relative growth (irradiated/un-irradiated) is significantly poorer for POLIE-depleted cells compared to uninduced cells (Supplementary Figure S2I). Therefore, POLIE appears to play an important role in EMS, UV, and cisplatin-induced DNA damage repair in *T. brucei*.

Since POLIE is a telomere protein, we further examined its role in telomere integrity. Western analysis detected no changes in the levels of TRF and RAP1, two telomere proteins (46,47), but an increased amount of γH2A, a marker of damaged DNA (76), upon POLIE depletion (Figure 2E). IF using a γH2A antibody (50) showed that >90% of POLIE-depleted and ∼10% uninduced POLIE RNAi cells exhibited a positive γH2A signal (Figure 2F). ChIP analysis using the γH2A antibody (50) showed that significantly more γH2A was associated with the telomere chromatin after depletion of POLIE (Figure 2G; S2J). In addition, we analyzed the γH2A ChIP product by quantitative PCR using primers specific to the active *VSG2*, silent *VSG16* and *mVSG531*, the 70 bp repeats in the active ES (70 bp BES), the 70 bp repeats in a silent ES (70 bp telo), rDNA, and a chromosome internal gene *SNAP50* (the latter two as controls). Depletion of POLIE resulted in an increased amount of γH2A associated with the subtelomere but not with chromosome internal loci (Figure 2H).

DNA double-strand breaks (DSBs) at or near the active *VSG* locus are a potent inducer for VSG switching (77,78). To estimate the VSG switching rate upon POLIE depletion (Supplementary Figure S3A), we introduced the POLIE RNAi construct into a strain specifically established for analyzing VSG switching (which we refer to as strain S) (63) to create S/IEi (Table 1). Because recovering VSG switchers relies on cell proliferation, we only induced POLIE RNAi for 30 h followed by removal of doxycycline from the medium by extensive washing. The S strain has a *puromycin resistance* (*PUR*) gene fused with a *thymidine kinase* (*TK*) gene immediately upstream of the active *VSG* (Supplementary Figure S3A). Switchers are expected to lose the TK ex-

pression and can be selected by ganciclovir (GCV) (79). Removal of doxycycline after 30 h of induction allowed cells to recover, and these cells were still responsive to doxycycline upon repeated treatment (Supplementary Figure S3B). As a control, we tagged one endogenous *POLIE* allele with the C-terminal 13× myc to establish the *POLIE*[+myc/+] S/IEi strain (Table 1). Western analysis showed depletion of POLIE-myc upon induction of POLIE RNAi and the recovery of the POLIE-myc protein level after removal of doxycycline (Supplementary Figure S3C). Transient depletion of POLIE resulted in an ∼3-fold higher VSG switching rate when compared to the S/ev control strain (Figure 2I), indicating that POLIE suppresses VSG switching. To confirm that this phenotype is specifically due to the depletion of POLIE, we established the S/IEi + ecPOLIE-myc strain that carries an ectopic *POLIE* allele (Table 1). Adding doxycycline induced both POLIE RNAi and the expression of the ectopic POLIE-myc (Supplementary Figure S3D). The VSG switching rate in S/IEi + ecPOLIE-myc cells is significantly lower than that in S/IEi cells and similar to that in S/ev cells when all cells were induced by doxycycline for 30 h (Figure 2I), confirming that the more frequent VSG switching phenotype was specifically caused by POLIE depletion. We also determined the VSG switching pathways in all obtained switchers (Supplementary Figure S3A). In the S/ev control cells, a small fraction of the switchers arose from *in situ* switch (5%) and crossover (10%), while *VSG* gene conversion (43%) and ES gene conversion/ES loss + *in situ* events (42%) were more popular (Figure 2J; Supplementary Figure S3A). In contrast, in cells depleted of POLIE, *in situ* switcher and crossover events were absent, a small fraction of switchers arose from ES gene conversion/ES loss + *in situ* events (12%), while *VSG* gene conversion became the predominant switching event (88%) (Figure 2J; Supplementary Figure S3A). Therefore, POLIE suppresses *VSG* gene conversion by maintaining telomere integrity.

We further examined the transcriptomic profile in POLIE-depleted cells. Total RNA was isolated from *POLIE*[+myc/+] RNAi cells after RNAi was induced for 0 and 30 h, and poly(A) RNA was enriched for making cDNA libraries followed by high throughput RNA sequencing analysis (Novogene Inc.). A small number of genes were either upregulated or downregulated upon depletion of POLIE (Supplementary Figure S4A). Most of the affected genes are *VSG*s (Supplementary Figure S4B), which was verified by quantitative RT-PCR (Supplementary Figure S4C). To verify that the upregulation of silent *VSGs* is not simply a consequence of more frequent VSG switching, we performed IF analysis and observed co-expression of originally silent VSG6 and VSG3 in individual cells upon POLIE depletion (Supplementary Figure S4D), strongly suggesting that POLIE depletion induced a true VSG derepression phenotype. We notice that VSG3 proteins have not been all deposited onto the cell surface, suggesting that it may be only mildly derepressed.

POLIE-depleted cells have an increased amount of telomeric circles and elongated telomere 3′ overhangs

We speculated that, in addition to suppressing subtelomere DNA recombination, POLIE may also suppress telomere recombination. Intratelomeric homologous recombination
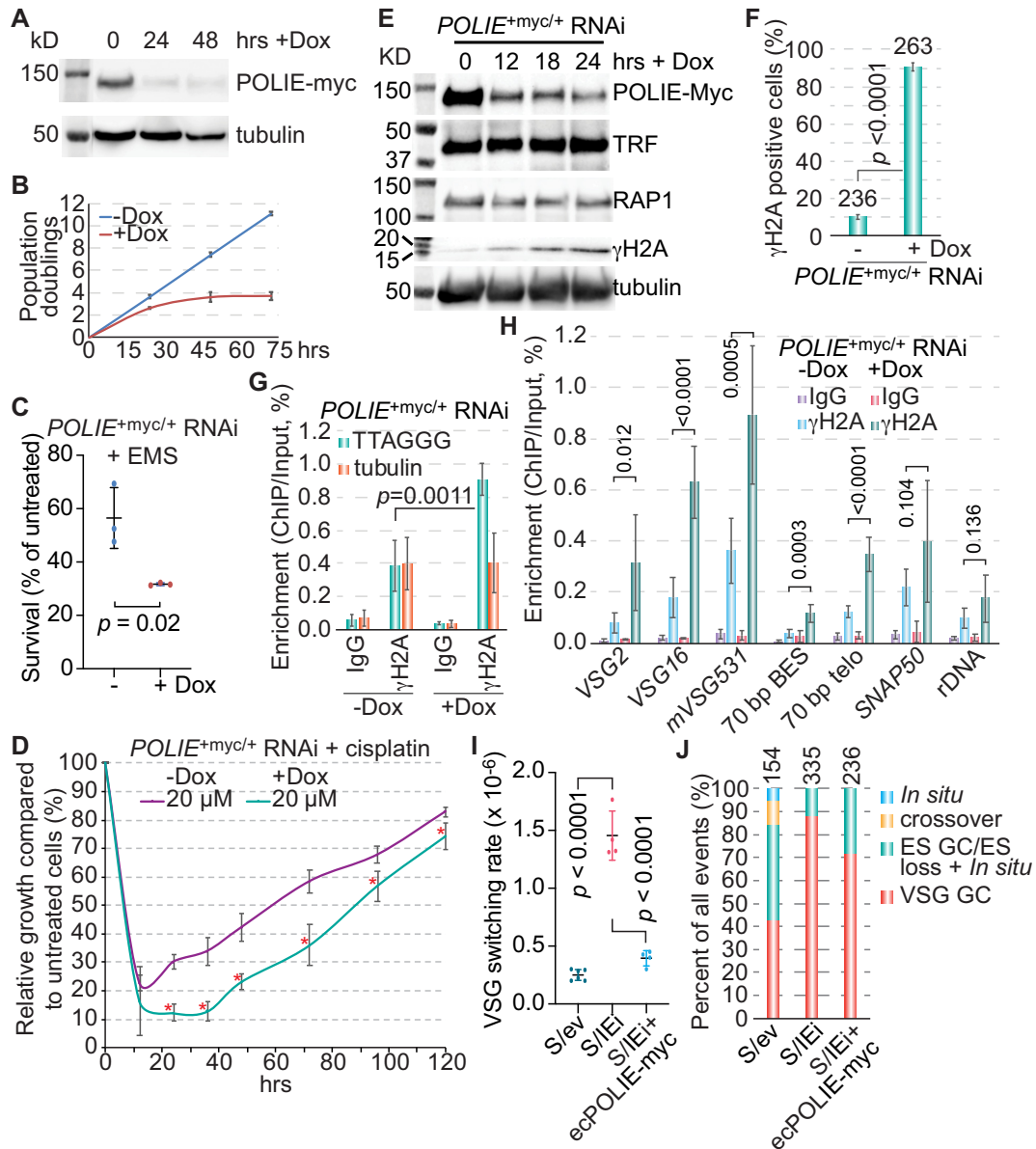
Figure 2. POLIE is essential for maintaining telomere integrity and suppresses VSG switching. (**A**) Western blotting showing depletion of POLIE-myc in *POLIE*[+myc/+] RNAi cells. (**B**) Growth curves of *POLIE*[+myc/+] RNAi cells without (–Dox) and with (+Dox) the induction of RNAi. (**C**) POLIE-depleted cells are more sensitive to EMS treatment. Survival of EMS-treated cells was calculated as a percentage of untreated cells with and without induction of POLIE RNAi by doxycycline. Average was calculated from three independent experiments. (**D**) *POLIE*[+myc/+] RNAi cells incubated with or without doxycycline for 12 h were treated with and without 20 µM cisplatin for 1 h before cells were washed free of doxycycline and cisplatin. Relative growth (treated/untreated) was calculated from three independent experiments. Asterisks indicate significant differences between relative growths of uninduced and induced cells. (**E**) Western blotting of whole cell lysate isolated from *POLIE*[+myc/+] RNAi cells before and after the induction of POLIE RNAi. The myc antibody 9E10, a TRF rabbit antibody (46), a RAP1 rabbit antibody (47), and a γH2A rabbit antibody (50) were used. (**F**) Quantification of the percent of *POLIE*[+myc/+] RNAi cells that are positive for the γH2A signal in IF before and after the induction of POLIE RNAi for 24 hrs. Total number of counted cells is indicated above each column. (**G**) Quantification of γH2A ChIP results. The average enrichment of γH2A at the telomere (ChIP/Input) was calculated from five independent experiments. (**H**) The γH2A ChIP products were analyzed by quantitative PCR using primers specific to various gene loci (indicated at the bottom), all of which except *rDNA* and *SNAP50* are at the subtelomere. The average enrichment of γH2A at each indicated locus was calculated from five to seven independent experiments. (**I**) VSG switching rates in the indicated strains. (**J**) Percent of various VSG switching mechanisms in the indicated strains. The total number of switchers characterized in each strain is listed on top of each column. *P*-values of unpaired *t*-tests are shown in (C), (F), (G), (H) and (I).

(HR), such as excision of the T-loop structure, can result in extra chromosomal telomeric circles (T-circles) (80). We performed 2D gel electrophoresis to separate circular from linear DNA molecules followed by Southern hybridization with a telomere probe. In uninduced POLIE RNAi cells, there is only a faint signal representing the telomere sequence-containing circular DNA (Figure 3A, B). After depletion of POLIE, the T-circle signal was much stronger (Figure 3A, C), suggesting that POLIE suppresses telomere recombination.

The active *VSG*-adjacent telomere is transcribed by RNA polymerase I into telomeric repeat-containing RNA (TERRA) in *T. brucei* (50,51). TERRA has a propensity to form the telomeric R-loop (TRL) (81), and we have shown that an excessive amount of TRL induces more frequent telomere/subtelomere recombination (50,51). Since POLIE depletion induced a mild VSG derepression (Supplementary Figure S4), we suspected that depletion of POLIE could also increase the TERRA level. To our surprise, we detected a lower level of TERRA after POLIE depletion in both Northern and slot blot hybridizations (Figure 3D–F). Therefore, it is unlikely that the increased level of telomere and subtelomere recombination is caused by an increased TRL level in POLIE-depleted cells.

The single-stranded telomere 3′ overhangs can invade a homologous sequence and induce HR (82). Therefore, we tested whether depletion of POLIE affected the telomere 3′ overhang structure. Using the native in-gel hybridization analysis, we detected a very faint telomere 3′ overhang signal in WT cells (Figure 4A), confirming our previous observations (44,45). Depletion of POLIE led to an ∼19-fold more intense telomere 3′ overhang signal (Figure 4A, C), which was sensitive to Exo I, a 3′ to 5′ ssDNA specific exonuclease (Figure 4A), indicating that the signal we detected was indeed from the telomere 3′ overhang. In addition, only the $(CCCTAA)_4$ probe detected overhang signals (Figure 4A), while the $(TTAGGG)_4$ probe did not (Figure 4B), confirming that the *T. brucei* telomere overhang has a G-rich sequence (44,45). We also performed Pulsed-Field Gel Electrophoresis (PFGE) to separate intact *T. brucei* chromosomes and performed the same native in-gel hybridization. Only G-rich telomere overhang signals were detected, and POLIE depletion again increased the intensity of the telomere 3′ overhang signal significantly (Supplementary Figure S5A). Furthermore, the EtBr-stained gel and the post-denaturation hybridization showed more smeary DNA species in POLIE-depleted cells than in WT and uninduced POLIE RNAi cells (Supplementary Figure S5A, left and right), further indicating that depletion of POLIE led to an increased amount of telomere DNA degradation. These observations suggest that POLIE normally suppresses the telomere recombination by limiting the length of the telomere 3′ overhang. As a control, we have also examined the telomere 3′ overhang structure in $POLIE^{+myc/-}$ and S/IEi + ecPOLIE-myc cells. As shown in Supplementary Figure S6, the telomere 3′ overhang level in $POLIE^{+myc/-}$ and S/IEi + ecPOLIE-myc cells are comparable to that in WT cells, indicating that POLIE-myc retains POLIE's key telomere function and that ectopic POLIE-myc can complement phenotypes in POLIE-depleted cells.

The telomerase-mediated telomere G-strand synthesis is expected to elongate the telomere 3′ overhang length (4). In addition, we previously found that the telomere 3′ overhang is lost in telomerase null *T. brucei* cells (45). To examine whether the elongated telomere 3′ overhang in POLIE-depleted cells depends on telomerase, we established the $TR^{-/-}$ POLIE RNAi strain (Table 1). Although the telomere 3′ overhang signal in uninduced $TR^{-/-}$ POLIE RNAi cells was essentially undetectable (Figure 4D, left), an ∼17-fold higher level of the telomere 3′ overhang signal was observed upon depletion of POLIE (Figure 4D, E). Similarly, PFGE of intact chromosomes followed by native in-gel hybridization showed the same elongated telomere 3′ overhang phenotype upon POLIE depletion in the $TR^{-/-}$ background (Supplementary Figure S5B, C). As expected, no $(TTAGGG)_4$ hybridization signal was detected in the $TR^{-/-}$ background, either (Figure 4D, right; Supplementary Figure S5C). Therefore, the elongated telomere 3′ overhang phenotype in POLIE-depleted cells is not dependent on the telomerase activity.

Depletion of POLIE increases telomere G-strand synthesis in a telomerase-dependent manner

WT *T. brucei* cells have very short telomere 3′ overhangs (44,45), suggesting that the telomere G- and C-strand synthesis is well-coordinated. To investigate how telomere 3′ overhangs were elongated in POLIE-depleted cells, we examined the telomere DNA synthesis. Labeling cells with BrdU for one cell cycle followed by CsCl gradient centrifugation should be able to separate the leading and lagging telomere DNA synthesis products, because one telomere strand has two Ts per TTAGGG repeat and the other strand one T per CCCTAA repeat (83). However, BrdU incorporation in *T. brucei* is frequently at very low efficiency (84) and appears to be toxic at a high level (85). In addition, although *T. brucei* cells can be arrested at the S phase by hydroxyurea (HU), they are poorly synchronized after HU release, possibly due to the atypical cell cycle control in these cells (86). Therefore, we used EdU-labeling to examine the telomere DNA synthesis in asynchronous cells, and most of the incorporated EdU signal is expected to result from DNA replication in the S phase. POLIE depletion leads to cell growth arrest by 24 h after induction, which interferes with the EdU incorporation. Hence, $POLIE^{+myc/+}$ RNAi cells were only induced 12 h before the cells were labeled with EdU for 3 h. EdU-labeled DNA was conjugated to desthiobiotin by the CLICK chemistry, pulled-down by streptavidin beads, and detected by hybridization with telomere and tubulin probes. Because the two telomere strands contain either G or C but not both, we used radioactive dCTP-labeled $(CCCTAA)_n$ and radioactive dGTP-labeled $(TTAGGG)_n$ probes to specifically detect the G- and C-strand telomere DNA, respectively. Depletion of POLIE did not affect tubulin DNA synthesis (Figure 5A, B; Supplementary Figure S7). Interestingly, POLIE-depletion resulted in a mild and significant increase in the telomere G-strand DNA synthesis (Figure 5A, B; Supplementary Figure S7). POLIE-depletion appeared to also decrease the telomere C-strand synthesis (Figure 5A, B; Supplementary Figure S7), but the decrease was not sig-
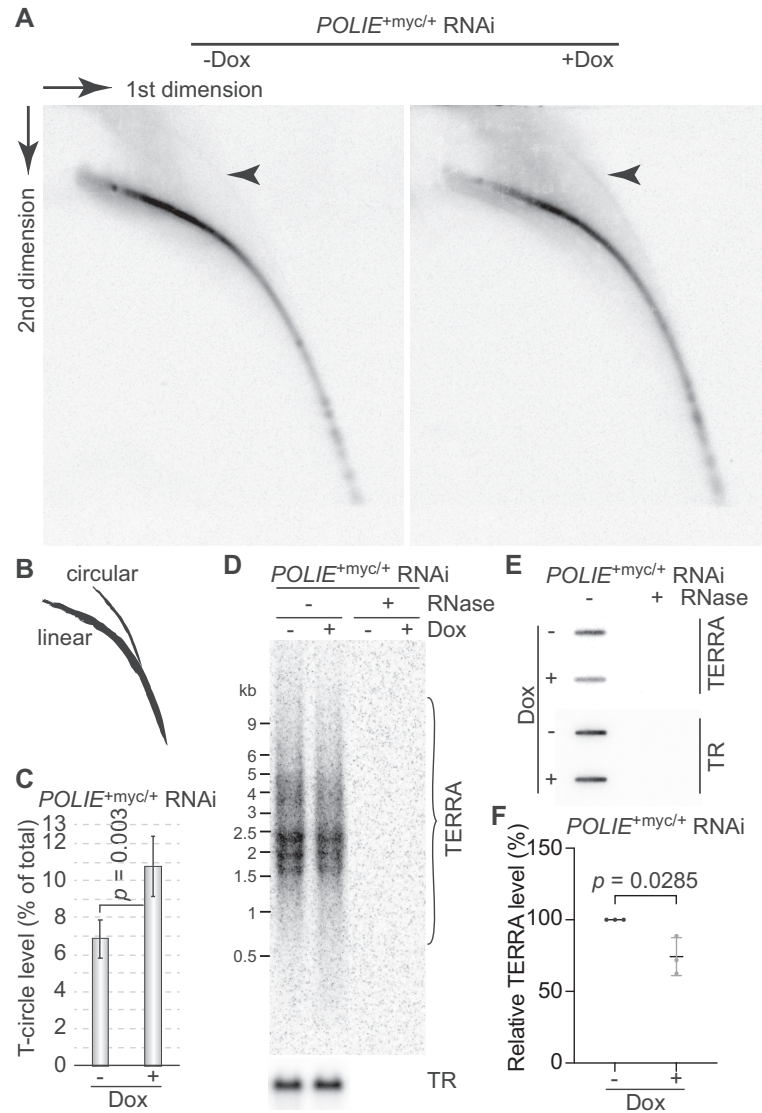
Figure 3. Depletion of POLIE leads to an increased amount of T-circles. (**A**) 2D gel electrophoresis of AluI/MboI digested genomic DNA isolated from *POLIE*^+myc/+ RNAi cells before (–Dox) and after (+Dox) 24-h of RNAi induction. Arrowheads indicate the circular telomere DNA. (**B**) A diagram showing expected migration patterns of linear and circular DNAs in 2D electrophoresis (60). (**C**) Quantification of Southern results after 2D electrophoresis. The average T-circle amount (percent of total telomeric DNA) was calculated from six independent experiments. (**D**) Northern hybridization detecting TERRA in *POLIE*^+myc/+ RNAi cells before (–Dox) and after (+Dox) the RNAi induction. The rRNA precursors are very abundant and shown as non-specific bands (three bands between 1.6 and 2.5 kb) overlapping with the TERRA species. The telomerase RNA component, TR, was detected as a loading control. (**E**) A representative slot blot detecting TERRA in *POLIE*^+myc/+ RNAi cells. TR was detected as a loading control. (**F**) Quantification of relative TERRA levels in *POLIE*^+myc/+ RNAi cells (normalized against the TR level). Average was calculated from three independent experiments. *P* values of unpaired *t*-tests are shown in (C) and (F).

nificantly different from that of the tubulin DNA (Figure 5B). We further performed telomere Southern analysis in *POLIE*^+myc/+ RNAi cells. However, within 24 h of POLIE RNAi induction, no significant telomere length change was observed (Figure 5C).

Telomerase can synthesize the telomere G-strand DNA *de novo*. To examine whether the increased level of telomere G-strand synthesis in POLIE-depleted cells is telomerase-dependent, we performed the EdU-labeling in *TR*^−/− POLIE RNAi cells. We found that POLIE depletion no longer increased the telomere G-strand synthesis in the TR null background (Figure 5D, E), indicating that the higher

level of the telomere G-strand synthesis was due to excessive telomerase-mediated telomere G-strand extension in POLIE-depleted cells. Therefore, POLIE is the first telomere protein in *T. brucei* that has been identified to suppress telomerase.

POLIE depletion increases the telomeric C-circle level

POLIE depletion may affect the telomere C-strand fill-in, but the EdU-labeling experiment was not sensitive enough to show a significant change (Figure 5A, B; Supplementary Figure S7). Therefore, we examined whether POLIE deple-
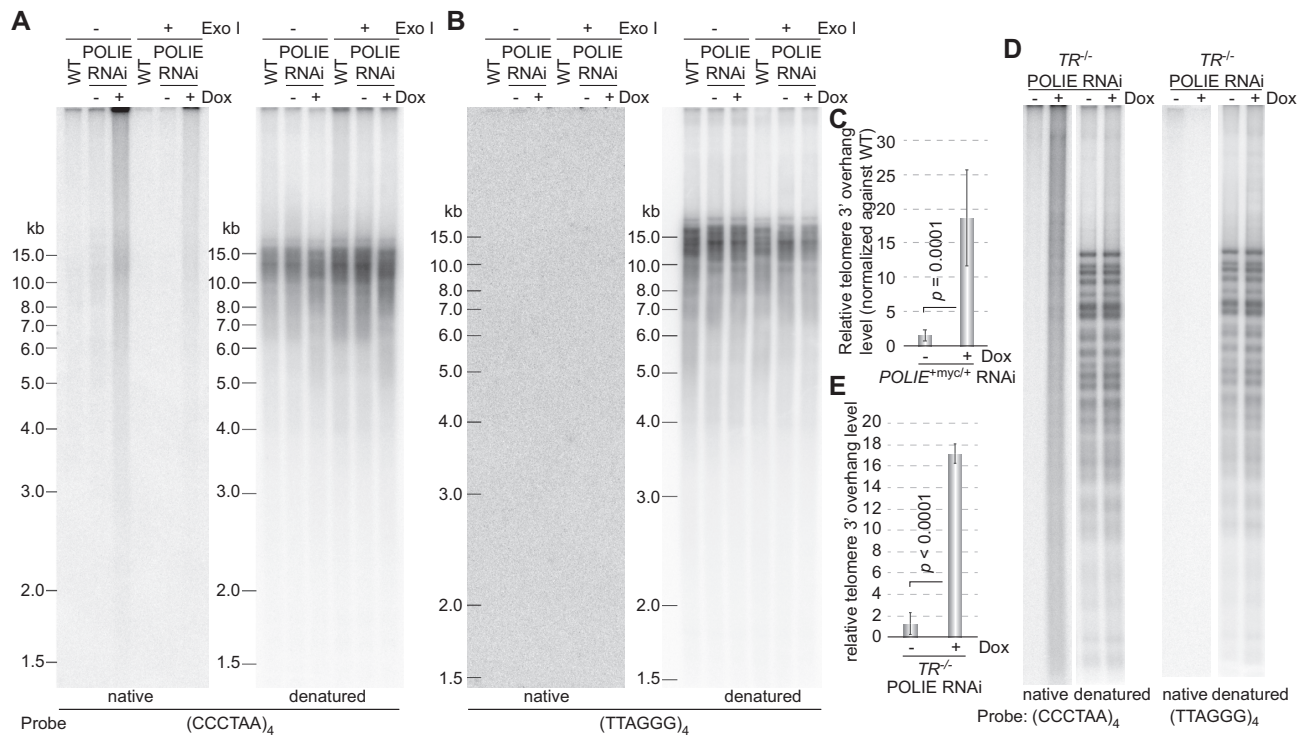
Figure 4. POLIE depletion results in longer telomere 3′ overhangs. Genomic DNAs were isolated from WT and *POLIE*$^{+myc/+}$ RNAi (labeled as POLIE RNAi) cells (**A, B**) or from *TR*$^{-/-}$ POLIE RNAi cells (**D**) before (–Dox) and after (+Dox) a 24-h induction of RNAi. The genomic DNA was treated with and without ExoI (NEB), which is a 3′ to 5′ single-strand DNA-specific exonuclease, and digested with AluI and MboI. In-gel hybridization was performed using a (CCCTAA)$_4$ or a (TTAGGG)$_4$ probe first under the native condition and then after denaturation and neutralization. The telomere 3′ overhang level is reflected by the hybridization intensity throughout the whole lane (excluding the signal in the well) but not by the sizes of the telomere fragments. (**C, E**) Quantification of the relative telomere 3′ overhang level (using the hybridization signal after the denaturation/neutralization as a loading control and using the telomere 3′ overhang level in WT cells as a reference) in *POLIE*$^{+myc/+}$ RNAi cells (C) and in *TR*$^{-/-}$ POLIE RNAi cells (E) before (-Dox) and after (+Dox) POLIE RNAi induction. The average telomere 3′ overhang level was calculated from three to six independent experiments. *P* values of unpaired *t*-tests are shown in (C) and (E).

tion affected the telomeric C-circle level, as defects in telomere C-strand replication can lead to an increased amount of telomeric C-circles (Supplementary Figure S8A) (87). We performed the Φ29 DNA polymerase-mediated telomeric C-circle assay (Supplementary Figure S8B), which does not amplify T-circles because both strands of T-circles have nicks (65). We found that POLIE depletion led to a 6.7-fold increase in the amount of telomeric C-circles but did not affect the telomeric G-circle level (Figure 6; Supplementary Figure S8B). In telomerase-negative ALT cancer cells, telomere recombination is a predominant mechanism of telomere length maintenance, and telomeric C-circles are a hallmark of telomere recombination and ALT activity (65). Therefore, we examined whether deleting the telomerase further increased the telomeric C-circle level in POLIE-depleted cells. Unexpectedly, *TR*$^{-/-}$ cells had a lower level of telomeric C-circles than WT cells (Figure 6), and uninduced *TR*$^{-/-}$ POLIE RNAi cells also had a lower level of telomeric C-circles than uninduced POLIE RNAi cells (Figure 6B). Therefore, deleting telomerase is not sufficient to make *T. brucei* more ALT-like. Importantly, depletion of POLIE induced a 4.8-fold increase in the telomeric C-circle level in the *TR*$^{-/-}$ background (Figure 6), indicating that the POLIE depletion-induced increase in the telomeric C-circle level is telomerase-independent.

DISCUSSION

POLIE was previously identified in a pull-down experiment using a telomere repeat-containing oligo and a TRF IP experiment (66). We have also identified POLIE in an independent F2H-TRF pull-down experiment (49). However, POLIE was not confirmed to be a telomere protein previously. We identify POLIE in both telomere PICh and TRF/TIF2 2-step IP. These observations, together with the IF, co-IP, and ChIP results, validate that POLIE is an intrinsic component of the *T. brucei* telomere complex and is localized at the telomere throughout the cell cycle. An earlier study showed that proteins of a number of silent VSGs can be detected in POLIE-depleted cells (67). However, it was not known whether different silent VSGs can be derepressed simultaneously in individual cells. Using IF analysis, we have shown that upon depletion of POLIE, previously silent VSGs were co-expressed in individual cells, indicating that VSG monoallelic expression was indeed disrupted. We have also measured the VSG switching rate in cells transiently depleted of POLIE and detected an increased amount of telomeric DNA damage upon POLIE depletion. Our observations further indicate that POLIE suppresses VSG switching by maintaining telomere integrity. Furthermore, in the current study, we characterize POLIE's key functions in telomere end processing and reveal an underlying mech-
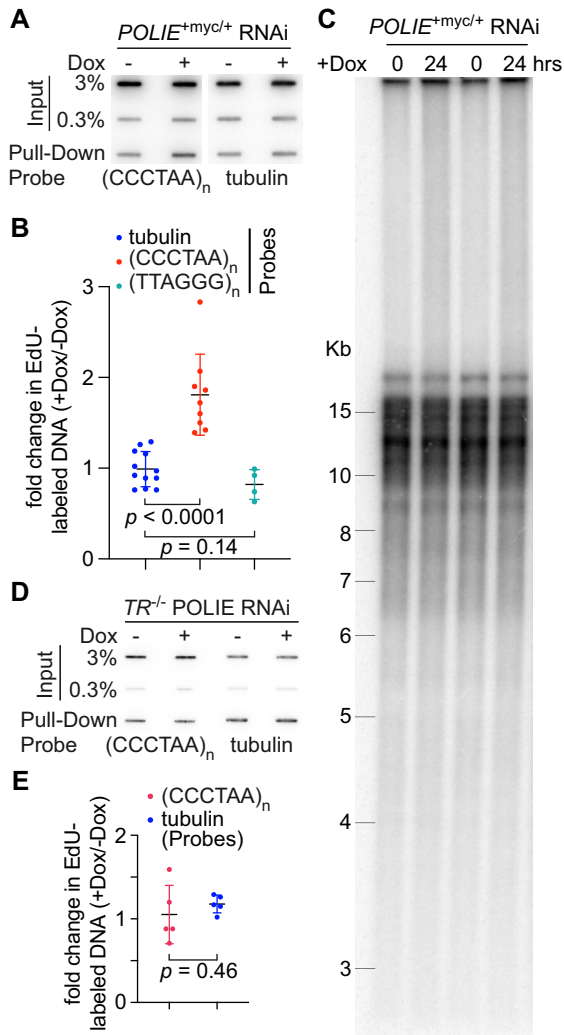
Figure 5. POLIE depletion increases the telomerase-mediated telomere G-strand synthesis. (A, D) In *POLIE*^+myc/+ RNAi (**A**) or *TR*^−/− POLIE RNAi (**D**) cells, before (–Dox) and after 12-h (+Dox) of POLIE RNAi induction, EdU-labeled nascent DNA was conjugated with desthiobiotin and pulled-down by streptavidin beads followed by slot blotting and hybridization using a telomere or a tubulin probe. The fold changes in the amount of EdU-labeled telomeric and tubulin DNA (+Doc/−Dox) were quantified and shown in (**B**) and (**E**), respectively. The average change was calculated from four to twelve independent experiments. *P* values of unpaired *t*-tests are shown in (**B**) and (**E**). (**C**) Depletion of POLIE did not affect the bulk telomere length within a short time frame. Genomic DNA isolated from *POLIE*^+myc/+ RNAi cells before (0 h) and after (24 h) POLIE RNAi induction were digested with AluI and MboI and separated by agarose gel electrophoresis. Southern blotting was performed using a telomere probe.

anism of how POLIE maintains telomere integrity and regulate VSG.

Depletion of POLIE decreases the TERRA level and increases the T-circle amount. However, the effects of POLIE on TERRA expression and telomere recombination is not a non-specific consequence of loss of viability. Depletion of RAP1 and TRF also leads to cell growth arrest but an elevated TERRA level (50,51). Therefore, cell growth arrest does not automatically lead to a lower level of TERRA. In addition, we can detect a low level of T-circles even in

WT cells, indicating that telomeric recombination can occur at a low level independent of cell growth defect. We have shown that *T. brucei* telomere proteins, including RAP1, TRF, and TIF2, affect VSG monoallelic expression and VSG switching (47–52,55,64). However, our current and previous work demonstrate that the underlying mechanisms of how POLIE and other telomere proteins regulate VSG are very different (see below).

Our first PICh in *T. brucei* successfully identified many telomere chromatin components. However, we still have not identified any OB-fold containing telomere-specific proteins, suggesting that *T. brucei* telomere complex has quite different protein components than those in higher eukaryotes. In mammals, yeasts, and plants, OB-fold containing telomere ssDNA binding proteins play critical roles in coordination of the telomere G- and C-strand syntheses. *T. brucei* lacks these OB-fold containing telomere-specific factors, suggesting that *T. brucei* uses a different mechanism to coordinate DNA syntheses of the two telomere strands and to regulate telomerase action at the telomere end. Indeed, our observations strongly suggest that POLIE is a novel telomere protein that suppresses telomerase-mediated telomere G-strand elongation and helps ensure proper telomere C-strand synthesis.

POLIE depletion increased the VSG switching rate and the amount of T-circles, indicating that POLIE suppresses DNA recombination at the telomere and subtelomere. POLIE-depleted cells have much longer telomere 3′ overhangs than WT cells, which likely contributes to the increased level of telomere recombination, as the long single-stranded 3′ overhang is prone to invade duplex DNA with a homologous sequence (82). The telomere 3′ overhang length depends on several factors (Figure 7), including the exonuclease-mediated resection of the telomere 5′ end, the telomerase-mediated telomere G-strand extension, and the telomere C-strand fill-in (4). Our results suggest that POLIE maintains a normal length of telomere 3′ overhang at at least two steps (Figure 7): EdU-labeling showed that POLIE-depleted cells have a significantly elevated level of telomere G-strand synthesis, which is telomerase-dependent, indicating that POLIE suppresses telomerase-mediated telomere G-strand extension. Considering that *T. brucei* telomeres are ∼15 kb long on average (Figure 5C) and the conventional DNA replication in the S phase contributes to the EdU-labeling signal considerably, even a mild increase in the telomere G-strand synthesis reflects a dramatically enhanced telomerase action at the telomere. POLIE is also likely required for telomere C-strand fill-in, which is supported by several observations. First, in telomerase null cells, depletion of POLIE still increases the telomere 3′ overhang length to a similar extent as that in the *TR*^+/+ background, suggesting that in addition to suppressing telomerase, POLIE also promotes the telomere C-strand fill-in. Second, we observed a mild decrease in telomere C-strand DNA synthesis upon POLIE depletion using the EdU-labeling assay, although this change is not significantly different from that of the tubulin DNA synthesis. This could be due to the fact that the EdU-labeling technique is not sensitive enough as asynchronous *T. brucei* cells were used. In addition, telomeres in the *T. brucei* cells used in this study are ∼15 kb long (Figure 5C). Hence,
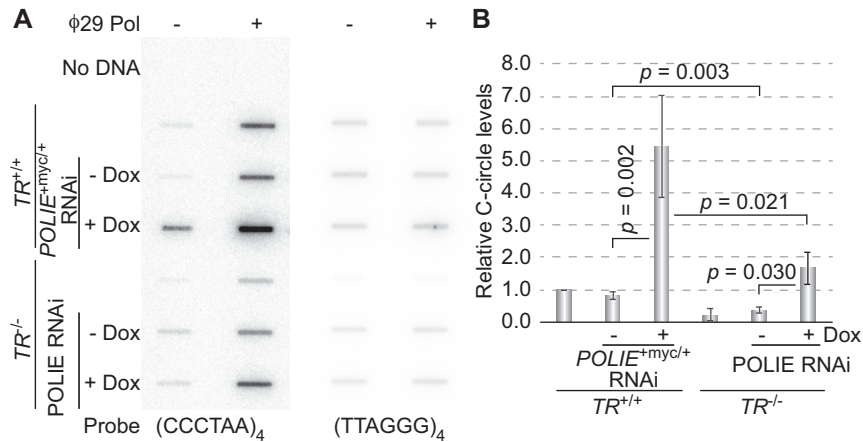
Figure 6. POLIE depletion increases the amount of telomeric C-circles, which is telomerase-independent. (**A**) The C-circle and G-circle products from indicated cells were detected in slot blot hybridization using a $(CCCTAA)_4$ and a $(TTAGGG)_4$ probe, respectively. (**B**) Quantification of the telomeric C-circle amount in the C-circle assay. The C-circle level in WT cells was arbitrarily set to 1, and relative C-circle levels in other cells were quantified using the WT level as a reference. The average C-circle signal level was calculated from three to four independent experiments. *P* values of unpaired *t*-tests are shown.
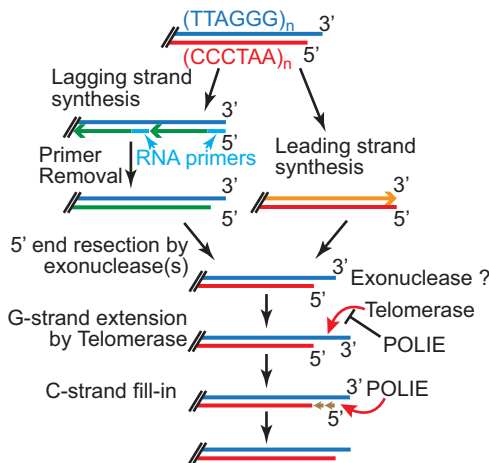
Figure 7. POLIE has essential functions in telomere end processes. Multiple processes are involved in the generation of a proper telomere 3' overhang structure. The exonuclease that resects the telomere 5' end has not been identified in *T. brucei*. Our observations suggest that POLIE suppresses the telomerase-mediated telomere G-strand elongation and is important for telomere C-strand fill-in.

the telomere C-strand fill-in is expected to have a limited contribution to the EdU incorporation. Third, POLIE depletion dramatically increases the telomeric C-circle level in a telomerase-independent manner, while telomeric C-circles can arise from telomere C-strand replication stress (87), further suggesting that POLIE is important for the telomere C-strand fill-in.

The inhibitory effects of POLIE on telomerase-mediated telomere G-strand extension and the positive effect of POLIE on telomere C-strand fill-in are unexpected. In mammalian, yeast, and plant cells, OB fold-containing proteins that bind the single-stranded telomere 3' overhang play important roles in coordinating the telomere G- and C-strand syntheses (25). Specifically, human TPP1 recruits telomerase to the telomere and stimulates telomerase activ-

ity (28–30), while binding of the CST complex on the telomere 3' overhang effectively inhibits telomerase-mediated telomere extension (31). In budding yeasts, CDC13, the single-stranded telomere DNA binding factor, both positively and negatively regulates telomerase-mediated telomere extension (32,33). Importantly, both vertebrate and yeast CST complexes promote the telomere C-strand fill-in by directly interacting with and recruiting DNA polymerase alpha-primase to the telomere (15,23,34–36). Therefore, single-stranded telomere DNA binding factors are major players to coordinate the synthesis of the two telomere strands. However, the *T. brucei* genome appears to lack these OB fold-containing telomere-specific ssDNA binding factors. On the other hand, our study identifies POLIE as an essential telomere maintenance factor that plays critical roles in coordinating the telomerase-mediated G-strand synthesis and C-strand fill-in. *T. brucei* POLIE is not only a novel telomerase regulator but also represents a completely new mechanism of telomere maintenance. Since POLIE is essential for *T. brucei* proliferation and regulates antigenic variation, our findings can also be applied to future development of anti-parasite agents.

DATA AVAILABILITY

All data are available in the main text or the supplementary materials. The RNAseq data have been deposited to GEO (GSE182941).

SUPPLEMENTARY DATA

Supplementary Data are available at NAR Online.

ACKNOWLEDGEMENTS

REFERENCES

1. Lim,C.J. and Cech,T.R. (2021) Shaping human telomeres: from shelterin and CST complexes to telomeric chromatin organization. *Nat. Rev. Mol. Cell Biol.*, **22**, 283–298.
2. de Lange,T. (2018) Shelterin-mediated telomere protection. *Annu. Rev. Genet.*, **52**, 223–247.
3. Podlevsky,J.D., Bley,C.J., Omana,R.V., Qi,X. and Chen,J.J. (2008) The telomerase database. *Nucleic Acids Res.*, **36**, D339–D343.
4. Bonetti,D., Martina,M., Falcettoni,M. and Longhese,M.P. (2014) Telomere-end processing: mechanisms and regulation. *Chromosoma*, **123**, 57–66.
5. Olovnikov,A.M. (1973) A theory of marginotomy. The incomplete copying of template margin in enzymic synthesis of polynucleotides and biological significance of the phenomenon. *J. Theor. Biol.*, **41**, 181–190.
6. Ohki,R., Tsurimoto,T. and Ishikawa,F. (2001) In vitro reconstitution of the end replication problem. *Mol. Cell. Biol.*, **21**, 5753–5766.
7. Greider,C.W. and Blackburn,E.H. (1987) The telomere terminal transferase of tetrahymena is a ribonucleoprotein enzyme with two kinds of primer specificity. *Cell*, **51**, 887–898.
8. Greider,C.W. and Blackburn,E.H. (1989) A telomeric sequence in the RNA of tetrahymena telomerase required for telomere repeat synthesis. *Nature*, **337**, 331–337.
9. Blackburn,E.H. and Collins,K. (2011) Telomerase: an RNP enzyme synthesizes DNA. *Cold Spring Harb. Perspect. Biol.*, **3**, a003558.
10. Schmidt,J.C. and Cech,T.R. (2015) Human telomerase: biogenesis, trafficking, recruitment, and activation. *Genes Dev.*, **29**, 1095–1105.
11. Tomáška,L., Cesare,A.J., AlTurki,T.M. and Griffith,J.D. (2020) Twenty years of t-loops: a case study for the importance of collaboration in molecular biology. *DNA Repair (Amst.)*, **94**, 102901.
12. Bonnell,E., Pasquier,E. and Wellinger,R.J. (2021) Telomere replication: solving multiple end replication problems. *Front. Cell Dev. Biol.*, **9**, 668171.
13. Wu,P., van Overbeek,M., Rooney,S. and de Lange,T. (2010) Apollo contributes to g overhang maintenance and protects leading-end telomeres. *Mol. Cell*, **39**, 606–617.
14. Keijzers,G., Liu,D. and Rasmussen,L.J. (2016) Exonuclease 1 and its versatile roles in DNA repair. *Crit. Rev. Biochem. Mol. Biol.*, **51**, 440–451.
15. Wu,P., Takai,H. and de Lange,T. (2012) Telomeric 3′ overhangs derive from resection by exo1 and apollo and fill-in by POT1b-associated CST. *Cell*, **150**, 39–52.
16. Wei,C. and Price,M. (2003) Protecting the terminus: t-loops and telomere end-binding proteins. *Cell. Mol. Life Sci.*, **60**, 2283–2294.
17. Takai,H., Jenkinson,E., Kabir,S., Babul-Hirji,R., Najm-Tehrani,N., Chitayat,D.A., Crow,Y.J. and de Lange,T. (2016) A POT1 mutation implicates defective telomere end fill-in and telomere truncations in coats plus. *Genes Dev.*, **30**, 812–826.
18. Arnoult,N., Saintome,C., Ourliac-Garnier,I., Riou,J.F. and Londoño-Vallejo,A. (2009) Human POT1 is required for efficient telomere C-rich strand replication in the absence of WRN. *Genes Dev.*, **23**, 2915–2924.
19. Aramburu,T., Plucinsky,S. and Skordalakes,E. (2020) POT1-TPP1 telomere length regulation and disease. *Comput. Struct. Biotechnol. J.*, **18**, 1939–1946.
20. Rajavel,M., Mullins,M.R. and Taylor,D.J. (2014) Multiple facets of TPP1 in telomere maintenance. *Biochim. Biophys. Acta*, **1844**, 1550–1559.
21. Feng,X., Hsu,S.J., Bhattacharjee,A., Wang,Y., Diao,J. and Price,C.M. (2018) CTC1-STN1 terminates telomerase while STN1-TEN1 enables C-strand synthesis during telomere replication in colon cancer cells. *Nat. Commun.*, **9**, 2827.
22. Gu,P., Jia,S., Takasugi,T., Smith,E., Nandakumar,J., Hendrickson,E. and Chang,S. (2018) CTC1-STN1 coordinates G- and C-strand synthesis to regulate telomere length. *Aging Cell*, **17**, e12783.
23. Feng,X., Hsu,S.J., Kasbek,C., Chaiken,M. and Price,C.M. (2017) CTC1-mediated C-strand fill-in is an essential step in telomere length maintenance. *Nucleic Acids Res.*, **45**, 4281–4293.
24. Amir,M., Khan,P., Queen,A., Dohare,R., Alajmi,M.F., Hussain,A., Islam,A., Ahmad,F. and Hassan,I. (2020) Structural features of nucleoprotein CST/Shelterin complex involved in the telomere maintenance and its association with disease mutations. *Cells*, **9**, 359–390.
25. Lue,N.F. (2018) Evolving linear chromosomes and telomeres: a C-strand-centric view. *Trends Biochem. Sci.*, **43**, 314–326.
26. Loayza,D. and de Lange,T. (2003) POT1 as a terminal transducer of TRF1 telomere length control. *Nature*, **424**, 1013–1018.
27. Lei,M., Podell,E.R. and Cech,T.R. (2004) Structure of human POT1 bound to telomeric single-stranded DNA provides a model for chromosome end-protection. *Nat. Struct. Mol. Biol.*, **11**, 1223–1229.
28. Nandakumar,J., Bell,C.F., Weidenfeld,I., Zaug,A.J., Leinwand,L.A. and Cech,T.R. (2012) The TEL patch of telomere protein TPP1 mediates telomerase recruitment and processivity. *Nature*, **492**, 285–289.
29. Zhong,F.L., Batista,L.F., Freund,A., Pech,M.F., Venteicher,A.S. and Artandi,S.E. (2012) TPP1 OB-fold domain controls telomere maintenance by recruiting telomerase to chromosome ends. *Cell*, **150**, 481–494.
30. Sandhu,R., Sharma,M., Wei,D. and Xu,L. (2021) The structurally conserved TELR region on shelterin protein TPP1 is essential for telomerase processivity but not recruitment. *Proc. Natl. Acad. Sci. U.S.A*, **118**, e2024889118.
31. Chen,L.Y., Redon,S. and Lingner,J. (2012) The human CST complex is a terminator of telomerase activity. *Nature*, **488**, 540–544.
32. Wu,Y. and Zakian,V.A. (2011) The telomeric cdc13 protein interacts directly with the telomerase subunit est1 to bring it to telomeric DNA ends in vitro. *Proc. Natl. Acad. Sci. U.S.A.*, **108**, 20362–20369.
33. Mersaoui,S.Y. and Wellinger,R.J. (2019) Fine tuning the level of the cdc13 telomere-capping protein for maximal chromosome stability performance. *Curr. Genet.*, **65**, 109–118.
34. Casteel,D.E., Zhuang,S., Zeng,Y., Perrino,F.W., Boss,G.R., Goulian,M. and Pilz,R.B. (2009) A DNA polymerase-{alpha}•primase cofactor with homology to replication protein A-32 regulates DNA replication in mammalian cells. *J. Biol. Chem.*, **284**, 5807–5818.
35. Huang,C., Dai,X. and Chai,W. (2012) Human stn1 protects telomere integrity by promoting efficient lagging-strand synthesis at telomeres and mediating C-strand fill-in. *Cell Res.*, **22**, 1681–1695.
36. Qi,H. and Zakian,V.A. (2000) The saccharomyces telomere-binding protein cdc13p interacts with both the catalytic subunit of DNA polymerase alpha and the telomerase- associated est1 protein. *Genes Dev.*, **14**, 1777–1788.
37. Cross,G.A.M., Kim,H.S. and Wickstead,B. (2014) Capturing the variant surface glycoprotein repertoire (the VSGnome) of *trypanosomabrucei* lister 427. *Mol. Biochem. Parasitol.*, **195**, 59–73.
38. de Lange,T. and Borst,P. (1982) Genomic environment of the expression-linked extra copies of genes for surface antigens of *trypanosomabrucei* resembles the end of a chromosome. *Nature*, **299**, 451–453.
39. Cross,G.A.M. (1975) Identification, purification and properties of clone-specific glycoprotein antigens constituting the surface coat of *trypanosomabrucei*. *Parasitology*, **71**, 393–417.
40. Dreesen,O., Li,B. and Cross,G.A.M. (2005) Telomere structure and shortening in telomerase-deficient *trypanosomabrucei*. *Nucleic Acids Res.*, **33**, 4536–4543.
41. Sandhu,R., Sanford,S., Basu,S., Park,M., Pandya,U.M., Li,B. and Chakrabarti,K. (2013) A trans-spliced telomerase RNA dictates telomere synthesis in *trypanosomabrucei*. *Cell Res.*, **23**, 537–551.
42. Gupta,S.K., Kolet,L., Doniger,T., Biswas,V.K., Unger,R., Tzfati,Y. and Michaeli,S. (2013) The *trypanosomabrucei* telomerase RNA (TER) homologue binds core proteins of the C/D snoRNA family. *FEBS Lett.*, **587**, 1399–1404.
43. Munoz-Jordan,J.L., Cross,G.A.M., de Lange,T. and Griffith,J.D. (2001) t-loops at trypanosome telomeres. *EMBO J.*, **20**, 579–588.
44. Sandhu,R. and Li,B. (2011) Examination of the telomere G-overhang structure in *trypanosomabrucei*. *J. Vis. Exp.*, **47**, 1959.

45. Sandhu,R. and Li,B. (2017) Telomerase activity is required for the telomere G-overhang structure in *trypanosomabrucei*. *Sci. Rep.*, **7**, 15983.

46. Li,B., Espinal,A. and Cross,G.A.M. (2005) Trypanosome telomeres are protected by a homologue of mammalian TRF2. *Mol. Cell. Biol.*, **25**, 5011–5021.

47. Yang,X., Figueiredo,L.M., Espinal,A., Okubo,E. and Li,B. (2009) RAP1 is essential for silencing telomeric variant surface glycoprotein genes in *trypanosomabrucei*. *Cell*, **137**, 99–109.

48. Jehi,S.E., Li,X., Sandhu,R., Ye,F., Benmerzouga,I., Zhang,M., Zhao,Y. and Li,B. (2014) Suppression of subtelomeric VSG switching by *trypanosomabrucei* TRF requires its TTAGGG repeat-binding activity. *Nucleic Acids Res.*, **42**, 12899–12911.

49. Jehi,S.E., Wu,F. and Li,B. (2014) *Trypanosoma brucei* TIF2 suppresses VSG switching by maintaining subtelomere integrity. *Cell Res.*, **24**, 870–885.

50. Nanavaty,V., Sandhu,R., Jehi,S.E., Pandya,U.M. and Li,B. (2017) *Trypanosoma brucei* RAP1 maintains telomere and subtelomere integrity by suppressing TERRA and telomeric RNA:DNA hybrids. *Nucleic Acids Res.*, **45**, 5785–5796.

51. Saha,A., Gaurav,A.K., Pandya,U.M., Afrin,M., Sandhu,R., Nanavaty,V., Schnur,B. and Li,B. (2021) *Tb*TRF suppresses the TERRA level and regulates the cell cycle-dependent TERRA foci number with a TERRA binding activity in its C-terminal myb domain. *Nucleic Acids Res.*, **49**, 5637–5653.

52. Afrin,M., Gaurav,A.K., Yang,X., Pan,X., Zhao,Y. and Li,B. (2020) *Tb*RAP1 has an unusual duplex DNA binding activity required for its telomere localization and VSG silencing. *Sci. Adv.*, **6**, eabc4065.

53. Benmerzouga,I., Concepcion-Acevedo,J., Kim,H.S., Vandoros,A.V., Cross,G.A.M., Klingbeil,M.M. and Li,B. (2013) *Trypanosoma brucei* orc1 is essential for nuclear DNA replication and affects both *VSG* silencing and *VSG* switching. *Mol. Microbiol.*, **87**, 196–210.

54. Hovel-Miner,G.A., Boothroyd,C.E., Mugnier,M., Dreesen,O., Cross,G.A.M. and Papavasiliou,F.N. (2012) Telomere length affects the frequency and mechanism of antigenic variation in *trypanosomabrucei*. *PLoS Pathog.*, **8**, e1002900.

55. Pandya,U.M., Sandhu,R. and Li,B. (2013) Silencing subtelomeric VSGs by *trypanosomabrucei* RAP1 at the insect stage involves chromatin structure changes. *Nucleic Acids Res.*, **41**, 7673–7682.

56. Saha,A., Nanavaty,V.P. and Li,B. (2019) Telomere and subtelomere R-loops and antigenic variation in trypanosomes. *J. Mol. Biol.*, **432**, 4167–4185.

57. Li,B. (2021) Keeping balance between genetic stability and plasticity at the telomere and subtelomere of *trypanosomabrucei*. *Front. Cell Dev. Biol.*, **9**, 699639.

58. Li,B. and Zhao,Y. (2021) Regulation of antigenic variation by *trypanosomabrucei* telomere proteins depends on their unique DNA binding activities. *Pathogens*, **10**, 967–986.

59. Milman,N., Motyka,S.A., Englund,P.T., Robinson,D. and Shlomai,J. (2007) Mitochondrial origin-binding protein UMSBP mediates DNA replication and segregation in trypanosomes. *Proc. Natl. Acad. Sci. U.S.A.*, **104**, 19250–19255.

60. Klebanov-Akopyan,O., Mishra,A., Glousker,G., Tzfati,Y. and Shlomai,J. (2018) *Trypanosoma brucei* UMSBP2 is a single-stranded telomeric DNA binding protein essential for chromosome end protection. *Nucleic Acids Res.*, **46**, 7757–7771.

61. Dejardin,J. and Kingston,R.E. (2009) Purification of proteins associated with specific genomic loci. *Cell*, **136**, 175–186.

62. Wirtz,E., Leal,S., Ochatt,C. and Cross,G.A.M. (1999) A tightly regulated inducible expression system for dominant negative approaches in *trypanosomabrucei*. *Mol. Biochem. Parasitol.*, **99**, 89–101.

63. Kim,H.S. and Cross,G.A.M. (2010) TOPO3alpha influences antigenic variation by monitoring expression-site-associated *VSG* switching in *trypanosomabrucei*. *PLoS Pathog.*, **6**, e1000992.

64. Afrin,M., Kishmiri,H., Sandhu,R., Rabbani,M.A.G. and Li,B. (2020) *Trypanosoma brucei* RAP1 has essential functional domains that are required for different protein interactions. *mSphere*, **5**, e00027-20.

65. Henson,J.D., Cao,Y., Huschtscha,L.I., Chang,A.C., Au,A.Y., Pickett,H.A. and Reddel,R.R. (2009) DNA C-circles are specific and quantifiable markers of alternative-lengthening-of-telomeres activity. *Nat. Biotechnol.*, **27**, 1181–1185.

66. Reis,H., Schwebs,M., Dietz,S., Janzen,C.J. and Butter,F. (2018) TelAP1 links telomere complexes with developmental expression site silencing in african trypanosomes. *Nucleic Acids Res.*, **46**, 2820–2833.

67. Leal,A.Z., Schwebs,M., Briggs,E., Weisert,N., Reis,H., Lemgruber,L., Luko,K., Wilkes,J., Butter,F., McCulloch,R. *et al.* (2020) Genome maintenance functions of a putative *trypanosomabrucei* translesion DNA polymerase include telomere association and a role in antigenic variation. *Nucleic Acids Res.*, **48**, 9660–9680.

68. Conway,C., McCulloch,R., Ginger,M.L., Robinson,N.P., Browitt,A. and Barry,J.D. (2002) Ku is important for telomere maintenance, but not for differential expression of telomeric *VSG* genes, in african trypanosomes. *J. Biol. Chem.*, **277**, 21269–21277.

69. Janzen,C.J., Lander,F., Dreesen,O. and Cross,G.A.M. (2004) Telomere length regulation and transcriptional silencing in KU80-deficient trypanosoma brucei. *Nucleic Acids Res.*, **32**, 6575–6584.

70. Cestari,I. and Stuart,K. (2015) Inositol phosphate pathway controls transcription of telomeric expression sites in trypanosomes. *Proc. Natl. Acad. Sci. U.S.A.*, **112**, E2803–E2812.

71. Narayanan,M.S. and Rudenko,G. (2013) TDP1 is an HMG chromatin protein facilitating RNA polymerase i transcription in african trypanosomes. *Nucleic Acids Res.*, **41**, 2981–2992.

72. Glover,L., Hutchinson,S., Alsford,S. and Horn,D. (2016) VEX1 controls the allelic exclusion required for antigenic variation in trypanosomes. *Proc. Natl. Acad. Sci. U.S.A.*, **113**, 7225–7230.

73. Rudd,S.G., Glover,L., Jozwiakowski,S.K., Horn,D. and Doherty,A.J. (2013) PPL2 translesion polymerase is essential for the completion of chromosomal DNA replication in the african trypanosome. *Mol. Cell*, **52**, 554–565.

74. Wood,R.D. and Doublié,S. (2016) DNA polymerase θ (POLQ), double-strand break repair, and cancer. *DNA Repair (Amst.)*, **44**, 22–32.

75. Moldovan,G.L., Madhavan,M.V., Mirchandani,K.D., McCaffrey,R.M., Vinciguerra,P. and D'Andrea,A.D. (2010) DNA polymerase POLN participates in cross-link repair and homologous recombination. *Mol. Cell. Biol.* **30**, 1088–1096.

76. Glover,L. and Horn,D. (2012) Trypanosomal histone gammaH2A and the DNA damage response. *Mol. Biochem. Parasitol.*, **183**, 78–83.

77. Boothroyd,C.E., Dreesen,O., Leonova,T., Ly,K.I., Figueiredo,L.M., Cross,G.A.M. and Papavasiliou,F.N. (2009) A yeast-endonuclease-generated DNA break induces antigenic switching in *trypanosomabrucei*. *Nature*, **459**, 278–281.

78. Glover,L., Alsford,S. and Horn,D. (2013) DNA break site at fragile subtelomeres determines probability and mechanism of antigenic variation in african trypanosomes. *PLoS Pathog.* **9**, e1003260.

79. Scahill,M.D., Pastar,I. and Cross,G.A.M. (2008) CRE recombinase-based positive-negative selection systems for genetic manipulation in *trypanosomabrucei*. *Mol. Biochem. Parasitol.*, **157**, 73–82.

80. Tomaska,L., Nosek,J., Kramara,J. and Griffith,J.D. (2009) Telomeric circles: universal players in telomere maintenance. *Nat. Struct. Mol. Biol.*, **16**, 1010–1015.

81. Toubiana,S. and Selig,S. (2018) DNA:RNA hybrids at telomeres - when it is better to be out of the (R) loop. *FEBS J.*, **285**, 2552–2566.

82. Haber,J.E. (2018) DNA repair: the search for homology. *Bioessays*, **40**, e1700229.

83. Chai,W., Du,Q., Shay,J.W. and Wright,W.E. (2006) Human telomeres have different overhang sizes at leading versus lagging strands. *Mol. Cell*, **21**, 427–435.

84. da Silva,M.S., Muñoz,P.A.M., Armelin,H.A. and Elias,M.C. (2017) Differences in the detection of BrdU/EdU incorporation assays alter the calculation for G1, s, and G2 phases of the cell cycle in trypanosomatids. *J. Eukaryot. Microbiol.*, **64**, 756–770.

85. Reynolds,D., Cliffe,L., Forstner,K.U., Hon,C.C., Siegel,T.N. and Sabatini,R. (2014) Regulation of transcription termination by glucosylated hydroxymethyluracil, base j, in *Leishmania major* and *Trypanosoma brucei*. *Nucleic Acids Res.*, **42**, 9717–9729.

86. McKean,P.G. (2003) Coordination of cell cycle and cytokinesis in *Trypanosoma brucei*. *Curr. Opin. Microbiol.*, **6**, 600–607.

87. Zhang,T., Zhang,Z., Shengzhao,G., Li,X., Liu,H. and Zhao,Y. (2019) Strand break-induced replication fork collapse leads to C-circles, C-overhangs and telomeric recombination. *PLoS Genet.*, **15**, e1007925.